

FULL PAPER

Open Access



# A polymeric composite protective layer for stable Li metal anodes

Suogang Guo<sup>1,3</sup>, Li Wang<sup>2\*</sup>, Yuhong Jin<sup>3</sup>, Nan Piao<sup>2</sup>, Zonghai Chen<sup>4</sup>, Guangyu Tian<sup>5</sup>, Jiangang Li<sup>1,6</sup>, Chenchen Zhao<sup>3</sup> and Xiangming He<sup>2,5\*</sup> 

## Abstract

Lithium (Li) metal is a promising anode for high-performance secondary lithium batteries with high energy density due to its highest theoretical specific capacity and lowest electrochemical potential among anode materials. However, the dendritic growth and detrimental reactions with electrolyte during Li plating raise safety concerns and lead to premature failure. Herein, we report that a homogeneous nanocomposite protective layer, prepared by uniformly dispersing  $\text{AlPO}_4$  nanoparticles into the vinylidene fluoride-co-hexafluoropropylene matrix, can effectively prevent dendrite growth and lead to superior cycling performance due to synergistic influence of homogeneous Li plating and electronic insulation of polymeric layer. The results reveal that the protected Li anode is able to sustain repeated Li plating/stripping for > 750 cycles under a high current density of  $3 \text{ mA cm}^{-2}$  and renders a practical specific capacity of  $2 \text{ mAh cm}^{-2}$ . Moreover, full-cell Li-ion battery is constructed by using  $\text{LiFePO}_4$  and protected Li as a cathode and anode, respectively, rendering a stable capacity after 400 charge/discharge cycles. The current work presents a promising approach to stabilize Li metal anodes for next-generation Li secondary batteries.

**Keywords:**  $\text{AlPO}_4$  nanoparticles, fluoride-co-hexafluoropropylene, Protective layer, Lithium metal anode, Secondary lithium batteries

## 1 Introduction

The increasing demand for portable electronics and electric vehicles stimulates the endless pursuit of high-energy-density batteries [1–6]. As promising next-generation batteries, Li/S and Li/ $\text{O}_2$  batteries deliver a high theoretical energy density of  $2600 \text{ Wh kg}^{-1}$  and  $3505 \text{ Wh kg}^{-1}$ , respectively. It is worth emphasizing that the superior performance of Li/S and Li/ $\text{O}_2$  batteries mainly relies on the merits of metallic lithium (Li) anode. However, the instability of Li/electrolyte interface and undesirable dendritic growth during Li plating/stripping lead to internal short-circuiting and successive thermal runaway, limiting the successful realization of lithium metal batteries (LMBs). Also, the formation of

dendrites results in the continuous growth of solid electrolyte interphase (SEI), consuming the liquid electrolyte and leading to premature failure of LMBs. Therefore, different strategies have been developed to inhibit dendrite growth and enhance the lifetime of LMBs [3–5, 7–37].

The uneven surface properties of Li anode, including exposed crystal facets, nonuniform surface composition and roughness, are the root cause of dendrite formation, leading to the uneven transference of Li-ions and nonuniform Li plating/stripping speed. Hence, the local current density is significantly increased, which leads to uneven Li deposition. It has been reported that the local current density can be reduced by using high-surface-area current collectors [38–47], which results in a significantly improved cycling performance. Hence, only a uniform and strong artificial SEI, instead of native SEI, can alter the fundamental self-amplifying behavior of dendritic growth [2, 26, 48–59]. Recently, several research groups aimed to artificially develop a stable SEI to protect Li

\*Correspondence: wang-l@tsinghua.edu.cn; hexm@tsinghua.edu.cn

<sup>2</sup> Institute of Nuclear & New Energy Technology, Tsinghua University, Beijing 100084, People's Republic of China

Full list of author information is available at the end of the article

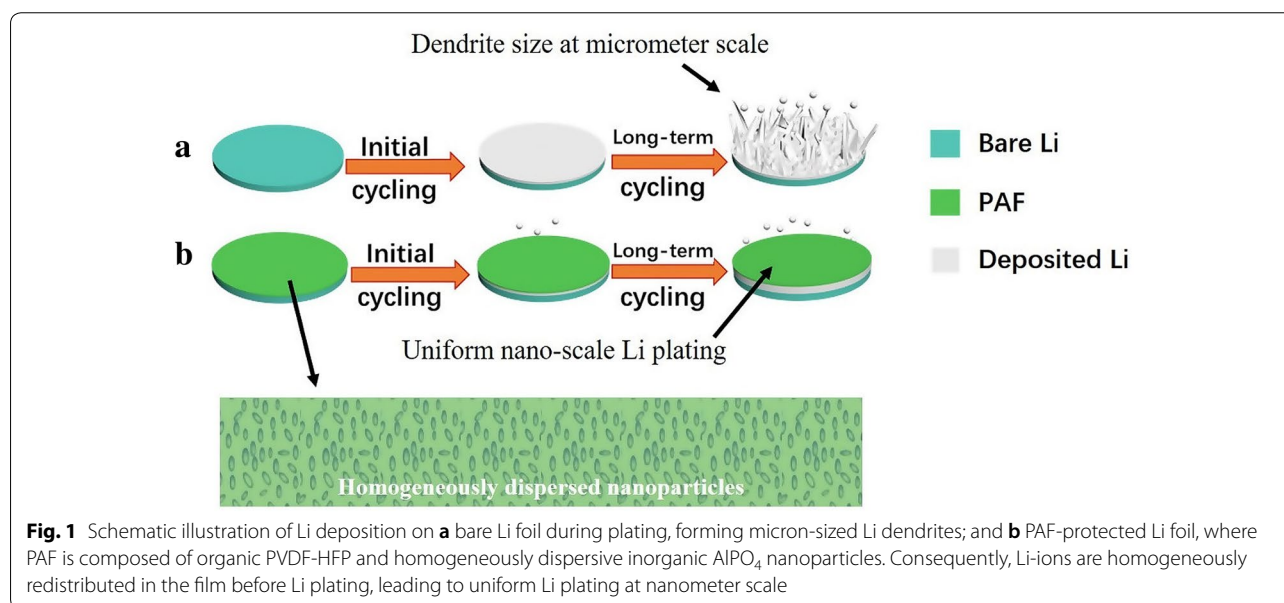
anode [48–53]. For instance, Huang's group [60] has prepared an artificial soft-rigid protective layer for dendrite-free Li anodes. It is worth noting  $\text{Al}_2\text{O}_3$  is a popular protective layer for battery applications [61–64]. In particular, the porous  $\text{Al}_2\text{O}_3$  layer, prepared by a facile spin-coating method, acts as a stable and dense interlayer to suppress side reactions between Li metal and electrolyte, and avoids the formation of surface cracks to suppress dendritic growth [62]. However, the inorganic  $\text{Al}_2\text{O}_3$  layers are relatively brittle and the construction method is cumbersome. The elastic moduli of protective layer is important [65]. Therefore, owing to the high elastic moduli of polymeric materials, polymeric SEI layers are being developed to protect Li metal anode and sustain volumetric changes during Li plating and stripping [24, 59, 66, 67]. However, the polymeric layers generally render inferior mechanical strength and ionic conductivity.

On the other hand, the composite artificial films are preferred due to their high ionic conductivity, low interface resistance and high mechanical modulus [3, 68]. Lee et al. [69] have designed an  $\text{Al}_2\text{O}_3$ /poly(vinylidene fluoride-co-hexafluoropropylene) (PVDF–HFP) composite layer to protect Li metal anode and demonstrated superior cycling performance in Li/ $\text{O}_2$  batteries. However,  $\text{Al}_2\text{O}_3$  exhibits poor stability in the electrolyte, transforming into  $\text{AlF}_3$  due to the presence of HF and lowering the ionic conductivity. Furthermore, it has been demonstrated that the uniformity of protective layer plays a critical role in inhibiting dendritic growth [3]. Therefore, a chemically and physically stable artificial SEI with high ionic conductivity should be designed to exploit the potential of Li metal anodes.

Nazar et al. have reported that the presence of an ionically conductive and electronically insulative layer on the surface of Li anode significantly suppresses the dendritic growth [70]. Zhang et al. [31, 71] have demonstrated that uniformly distributed Li-ions effectively eliminate the dendrites and lead to dendrite-free Li deposition. The size of Li dendrites is in the range of micrometers [29, 72–74], which implies that the growth of Li dendrites can be suppressed by nanoscale Li plating [75–78]. Previously, we have reported a novel route to uniformly disperse nanoparticles into polymeric solutions [79–83], enhancing the electrochemical performance of LIBs.

Nano- $\text{AlPO}_4$  composite prepared by organic ligand coordination is reported in our previous publication [84], showing good dispersion in a solution. This inspires us to prepare well-dispersed nano- $\text{AlPO}_4$  composite film to protect lithium anode. Moreover, a LiF coating layer can be formed via an in situ reaction between Li metal and PVDF–DMF solution to protect lithium metal anode [85].

Therefore, we propose a facile process to protect Li anode by forming a well-dispersed nano- $\text{AlPO}_4$ /PVDF–HFP composite film (PAF), rendering good homogeneity and nano-scale uniformity. The results demonstrate that the proposed method effectively suppresses the dendrite growth and leads to superior cycling performance of Li metal anodes. It is worth emphasizing that the usual size of Li dendrites ranges from 1 to 3  $\mu\text{m}$ , as shown in Fig. 1a [29, 72–74]. Owing to homogeneously dispersed nanoparticles in as-proposed PAF, Li-ions are homogeneously redistributed at the nanometer scale and lead to uniform Li-ion plating (Fig. 1b) [32].



## 2 Experimental

### 2.1 Preparation of PVDF-HFP/AlPO<sub>4</sub> film

#### 2.1.1 Preparation of AlPO<sub>4</sub> gel-solution

First, Al(NO<sub>3</sub>)<sub>3</sub>·9H<sub>2</sub>O was dissolved in ethanol and mixed with an appropriate amount of P<sub>2</sub>O<sub>5</sub> in a nitrogen-filled glovebox. The mixed solution was magnetically stirring at 50 °C for 3 h and filtered to collect the supernatant. The supernatant was placed in a water bath at 50 °C and an appropriate amount of (NH<sub>4</sub>)<sub>2</sub>CO<sub>3</sub> was completely dissolved by stirring. Then, the mixture was naturally cooled to room temperature and centrifuged at 5000 rpm for 10 min. Finally, the supernatant was separated and diluted with ethanol to obtain the AlPO<sub>4</sub> concentration of ~8 wt%.

#### 2.1.2 Fabrication of composite film

First, 0.1 g of PVDF-HFP was dissolved in 5 g of acetone and magnetically stirred for 5 h. Then, 1.25 g of as-prepared AlPO<sub>4</sub> solution was added into the above mixture and stirred for another 5 h. The obtained mixture was coated on a smooth glass plate with a defined thickness (5 μm). After room-temperature evaporation, the film was peeled-off and cut into circular discs with a diameter of 18 mm. The optimal mass portion of AlPO<sub>4</sub> in the composite film is 2%.

### 2.2 Electrochemical characterization

CR2032-type coin cells were assembled in an Ar-filled glovebox with water and oxygen content of <2 ppm. The coin cells were fabricated by stacking Li foil, PAF-protected Li foil and Celgard2400 separator. The electrochemical characterization was carried out by using Land Battery Tester (CT2001A, Wuhan LAND Electronics Co., Ltd., China). Li|Li and Li|PAF-Li symmetric batteries were cycled at the current densities of 0.5, 2, 3 and 5 mA cm<sup>-2</sup> in an ether-based electrolyte, i.e., 1.0 mol L<sup>-1</sup> lithium bis(trifluoromethanesulfonyl) imide (LiTFSI) dissolved in 1,3-dioxolane (DOL)/1,2-dimethoxyethane (DME) (v/v = 1:1) with 1.0 wt% lithium nitrate (LiNO<sub>3</sub>). The capacity of Li plating/stripping was controlled at 1 mAh cm<sup>-2</sup> or 2 mAh cm<sup>-2</sup>. The full-cell LIBs were constructed by using commercial LiFePO<sub>4</sub> (LFP) cathode and 1.0 M LiPF<sub>6</sub>-EC/DEC electrolyte. The LFP cathode was prepared by mixing 0.8 g of LFP powder, 0.1 g of Super P conductive carbon black and 1 g of PVDF (10 wt%) binder in NMP solvent. The slurry was coated on Al foil and dried at 60 °C for 2 h, followed by vacuum drying at 120 °C for 12 h. Then, the cathode was pressed by using Rolling Machine (MSK-2150) and punched into circular discs with a diameter of 13.0 mm. The average mass loading of LFP on each disk was ~3.4 mg cm<sup>-2</sup>.

### 2.3 Material characterization

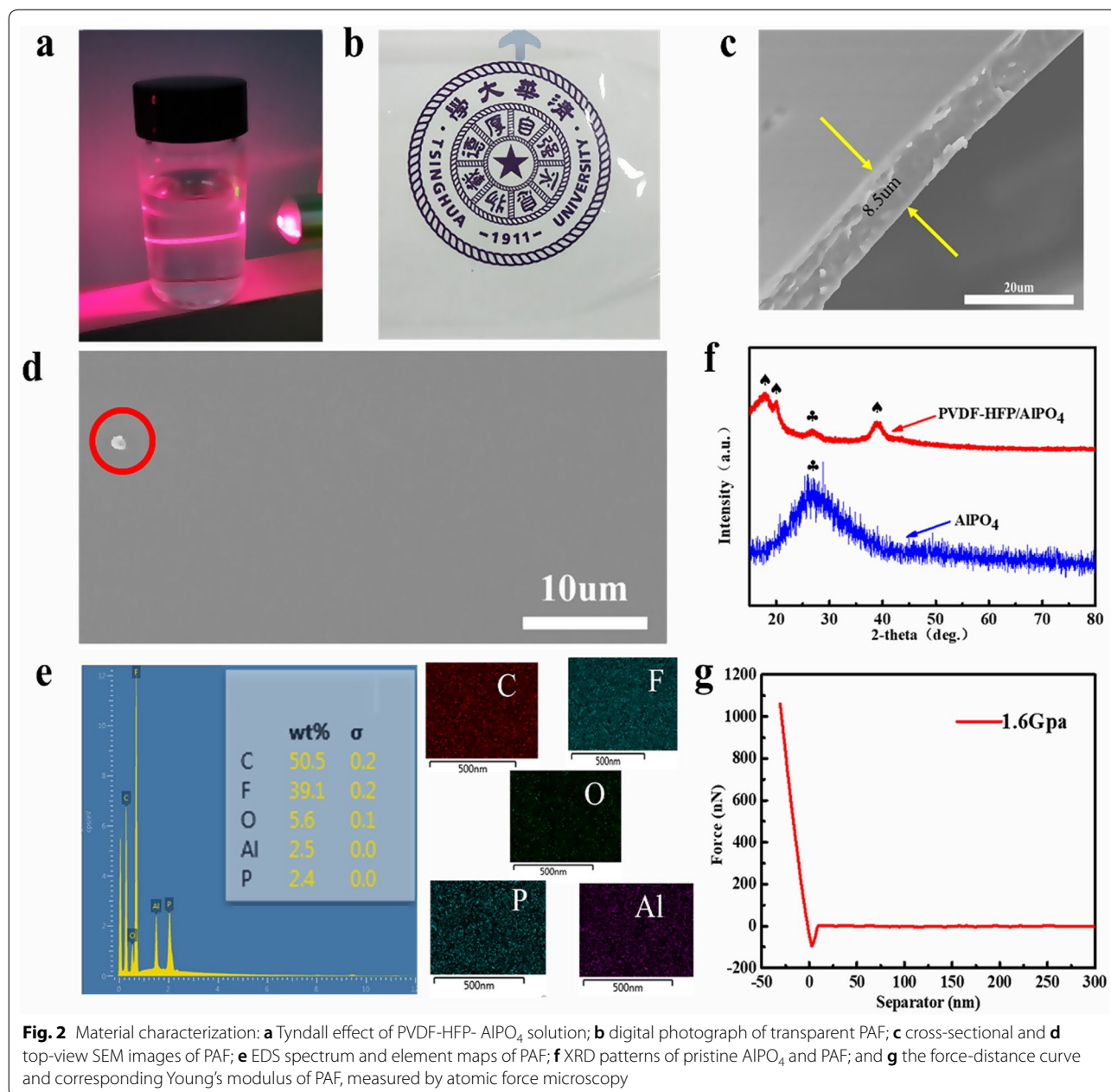
The surface morphology of different Li foils was observed by using a scanning electron microscope (SEM, Hitachi S-4800, Japan). The Young's modulus of PVDF-HFP/AlPO<sub>4</sub> composite film was measured by using atomic force microscopy (Bruker Multimode 8 with a Nanoscope V controller) in a N<sub>2</sub>-filled glovebox. X-ray diffraction (XRD) patterns were recorded by using a Rigaku D/MAX 2500/PC X-ray diffractometer, equipped with Cu Kα radiations (λ = 0.154 nm).

## 3 Results and discussion

Herein, PVDF-HFP is employed due to its excellent film-forming properties and utilization of PVDF-HFP-plasticizer-lithium salt system as a gel electrolyte for LIBs, which can be ascribed to the high Li-ion conductivity at room temperature and good electrochemical stability [86–89]. One should note that PVDF-HFP is a semi-crystalline polymer and the amorphous regions contribute to Li-ion conductivity, whereas crystalline regions ensure mechanical strength [60].

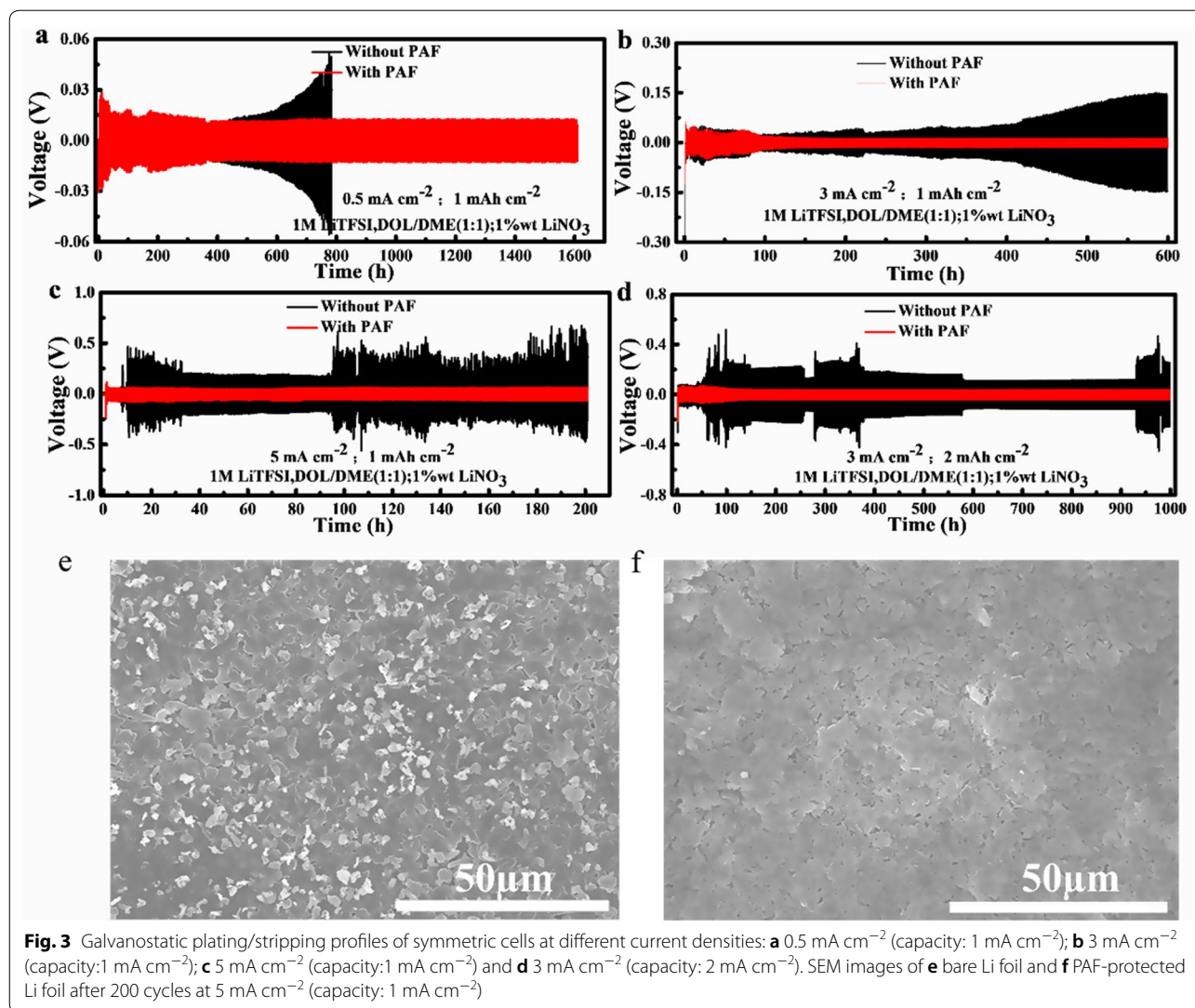
Figure 2a presents that the as-prepared PVDF-HFP/AlPO<sub>4</sub> solution exhibits a bright pathway under the action of a laser beam, which is referred as the Tyndall effect and indicates that nanoparticles are well-dispersed in the solution. The as-prepared film is shown in Fig. 2b, exhibiting a transparent appearance and clear texture. It can be concluded that the high content of AlPO<sub>4</sub> (10 wt%) did not deteriorate the uniformity of PAF, which can be attributed to the homogenous dispersion of nano-sized AlPO<sub>4</sub> in PVDF-HFP. Furthermore, SEM analysis was carried out to observe the uniformity and flatness of PAF. Figure 2d shows that the film surface is smooth and uniform without any obvious particles or protrusions. The particles, marked by a red-colored circle, correspond to accidentally-deposited dust during film preparation. Moreover, the uniform distribution of AlPO<sub>4</sub> in PAF can be further confirmed by energy dispersive spectroscopy (EDS). Figure 2e shows uniformly distributed carbon (C) and fluorine (F) elements, originating from PVDF-HFP, whereas oxygen (O), phosphorus (P) and aluminum (Al) represent the presence of AlPO<sub>4</sub>. The weight proportion of O, Al and P was 5.6%, 2.5% and 2.4%, respectively, corresponding to a molar ratio of 4.11:0.95:1.04 (AlPO<sub>4</sub>).

Figure 2f shows XRD patterns of AlPO<sub>4</sub> powder and PVDF-HFP/AlPO<sub>4</sub> composite film. The diffraction peaks, located at 2θ = 27.5°, correspond to amorphous phase of AlPO<sub>4</sub>. The diffraction peaks, located at 2θ = 17.9° and 20.0°, correspond to α-phase of PVDF-HFP, whereas the diffraction peak, located at 2θ = 38.9°, represents β-phase PVDF-HFP [90, 91]. XRD results confirm that PAF is a physical mixture of PVDF-HFP and AlPO<sub>4</sub>. In addition,



the modulus of inorganic  $\text{AlPO}_4$  is relatively high. Herein,  $8.5 \mu\text{m}$  (Fig. 2c) thick PAF film exhibited Young's modulus of  $1.6 \text{ GPa}$  (Fig. 2g), which can be ascribed to the presence of  $\text{AlPO}_4$ . On the other hand, Young's modulus of PVDF-HFP film ( $12 \mu\text{m}$ ) is only  $0.8 \text{ GPa}$  [60], which is far lower than the PAF but significantly higher than a typical SEI in LIBs ( $\approx 150 \text{ MPa}$ ) [55]. Therefore, the as-prepared PAF, with higher Young's modulus, is expected to inhibit the growth of Li dendrites during charge/discharge cycling.

Briefly, PAF is expected to work as a passivation layer and minimize the side reactions between metallic Li and liquid electrolyte. Consequently, symmetrical cells, with PAF-protected Li anodes, outperformed the symmetrical cells with bare Li at different current densities (Fig. 3a–d). The PAF-protected Li anode exhibited long-term cycling of up to 1600 h at a low current density of  $0.5 \text{ mA cm}^{-2}$ . As shown in Fig. 3a, PAF-protected Li anode exhibits higher electrochemical stability with lower voltage hysteresis than the bare Li electrode. The overpotential of the bare Li anode started to gradually



increase after 125 cycles (500 h), whereas the overpotential of PAF-protected Li anode remained stable even after 4000 cycles (1000 h). After 1600 h of charge/discharge time, the overpotential (281 mV) of the bare Li anode is found to be 3 times higher than the PAF-protected Li anode (87 mV). When the current density was increased to  $3 \text{ mA cm}^{-2}$ , the overpotential of bare Li anode started to gradually increase after 100 h and exhibited an overpotential of 147.9 mV after 600 h.

Such a huge hysteresis indicates the formation of a highly resistive interfacial layer, consisting of dead Li and the consumed electrolyte, which lead to continuous breaking and reconstruction of the SEI layer. On the other hand, the overpotential of PAF-protected Li anodes remained lower than 13 mV during the initial 600 h of operation, which is consistent with the low current

density. The lower overpotential and stable performance can be attributed to the protection of Li anode by PAF.

Interestingly, the phenomenon became more prominent at higher current densities, i.e.,  $5 \text{ mA cm}^{-2}$  (Fig. 3c). Under such a high current rate of  $5 \text{ mA cm}^{-2}$ , the cell voltage of bare Li anode rapidly increased after 25 cycles and remained unstable during subsequent cycles, whereas PAF-protected Li anode still exhibited a low polarization voltage (61 mV) after 500 cycles (200 h). Moreover, the cell with PAF-protected Li anode delivered a high areal capacity of  $2 \text{ mA h cm}^{-2}$  at the current density of  $3 \text{ mA cm}^{-2}$ , which shows better performance than the bare Li anode. Figure 3e, f present SEM images of bare and PAF-protected Li anodes, respectively, after 200 cycles at a current density of  $5 \text{ mA cm}^{-2}$  and a plating/stripping capacity of  $1 \text{ mA h cm}^{-2}$ . The SEM image of bare Li anode shows several particles on the surface of

(See figure on next page.)

**Fig. 4** Electrochemical performance of full-cell LIBs and SEM images of cycled Li metal anodes: long-term cycling stability at **a, c** 1 C and **b** 2 C; **d** galvanostatic charge–discharge profiles at 1st, 100th, 150th and 200th cycle; SEM images of **e, f** bare Li and **g, h** PAF-protected Li foils after 200 charge/discharge cycles

Li foil after cycling, indicating the deposition of a large amount of dead lithium and some Li dendrites. However, the PAF-protected Li anode did not show the dead Li or dendrites after electrochemical cycling (Fig. 3f).

Furthermore, we have assembled full-cell LIBs by using LFP, as a cathode, and PAF-protected Li metal, as an anode, to demonstrate the potential of using the proposed coating methodology in practical applications. Figure 4 shows the cycling performance of full-cell LIB and morphology of Li anode after charge/discharge cycling. Figure 4a, b present the cycling performance of Li|LFP and PAF-Li|LFP full-cells, respectively, at the 1 C and 2 C (1 C = 140 mAh g<sup>-1</sup>). The Li|LFP full-cell LIB delivered an initial specific capacity of 148.1 mAh g<sup>-1</sup> at 1 C, however, the capacity drastically decreased to 118 mAh g<sup>-1</sup> after 150 charge/discharge cycles, corresponding to a capacity retention of 79.7%. One should note that Li|LFP full-cell LIB exhibited a capacity of 52.2 mAh g<sup>-1</sup> after 240 charge/discharge cycles. However, PAF-Li|LFP full-cell LIB rendered an initial specific capacity of 154.3 mAh g<sup>-1</sup> at 1 C, which is slightly higher than the Li|LFP full-cell LIB, and retained 90% of the initial capacity after 400 charge/discharge cycles (140 mAh g<sup>-1</sup>).

Furthermore, we have carried out an interesting experiment, where the full-cell LIBs were galvanostatically cycled at 1 C and shelf-stored for 3 days after the 49th cycle. Interestingly, both full-cell LIBs exhibited a capacity drop. The drop in discharge capacity of Li|LFP full-cell LIB is significantly lower than the drop in discharge capacity of PAF-Li|LFP full-cell LIB. Subsequently, the capacity of Li|LFP full-cell LIB started to rapidly decrease after the 49th cycle, whereas the capacity of PAF-Li|LFP full-cell LIB is restored to the pre-49th cycle value (Fig. 4c). This shows the promise of PAF in maintaining the cycling stability of full-cell LIBs.

Moreover, the voltage curves show that both full-cell LIBs exhibit the same polarization voltage (92.7 mV) during the initial cycle (Fig. 4d). Similarly, after 100 charge/discharge cycles, the polarization voltage of both full-cell LIBs exhibits similar values. However, Li|LFP full-cell LIB shows a large polarization voltage of 153.7 mV and 313.8 mV after 150 and 200 cycles, respectively, whereas the PAF-Li|LFP full-cell LIB still exhibits a low polarization voltage of 109.8 mV after 200 cycles, corresponding to low interfacial resistance of PAF-protected Li anode. The surface morphology (Fig. 4 e–h) of electrochemically-cycled Li anode, after 230 charge/discharge

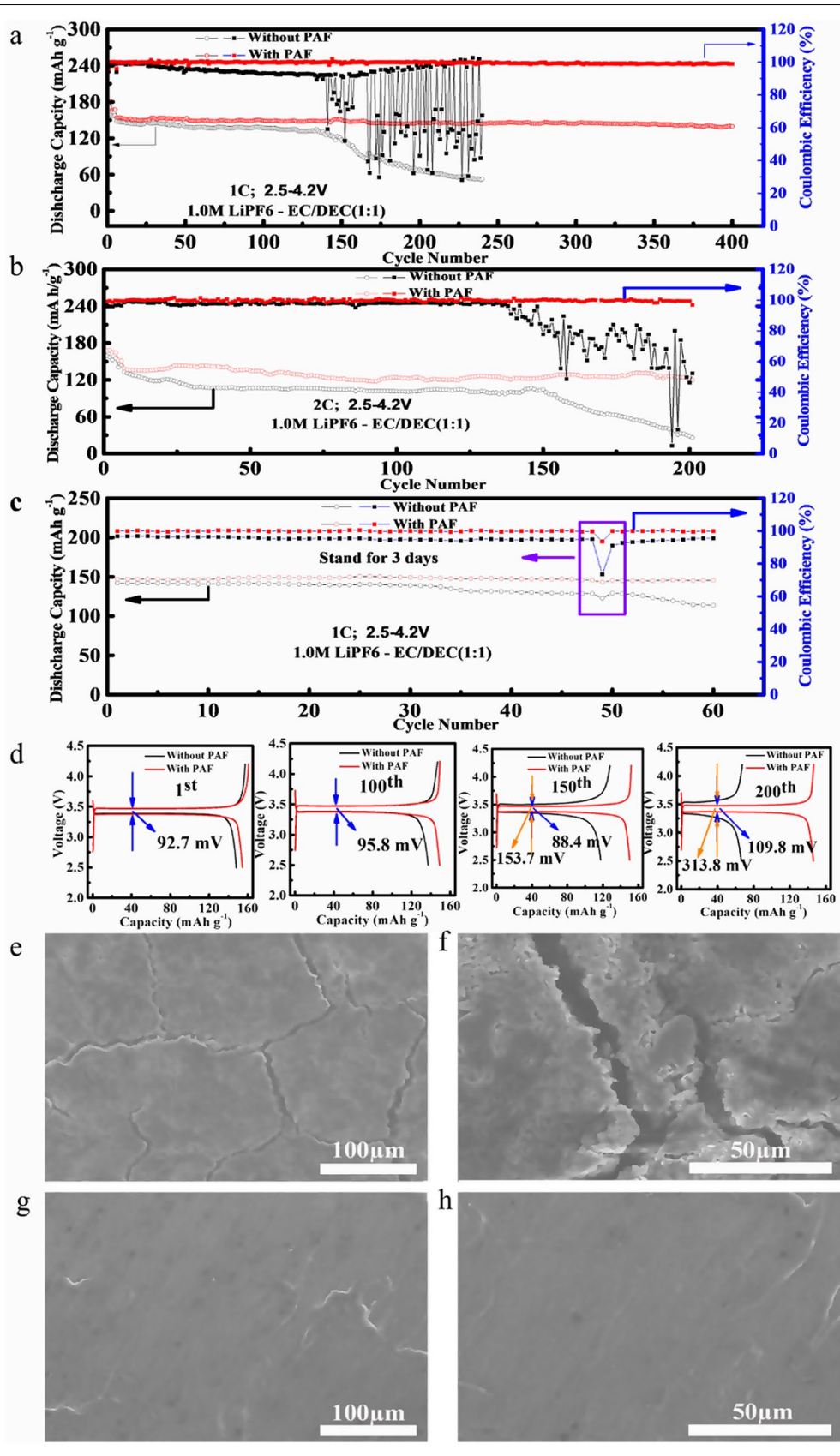
cycles, shows that the rough surface of bare Li foil possesses a large number of cracks (Fig. 4e, f), whereas PAF-protected Li foil exhibits a smooth and dense surface (Fig. 4g, h). One should note that the presence of PAF protective layer avoids the consumption of metallic Li due to side reactions between Li and electrolyte during long-term cycling.

Therefore, we have also carried out electrochemical impedance spectroscopy to understand the charge transfer kinetics of Li and PAF-protected Li anodes, as shown in Fig. 5. It should be noted that the high-frequency semicircle represents the interfacial resistance at the electrode/electrolyte interface, which also reflects the stability of SEI layer. Prior to electrochemical cycling, the PAF-Li|LFP full-cell LIB exhibits a higher interfacial resistance of 64 Ω, whereas Li|LFP full-cell LIB exhibits an interfacial resistance of only 55 Ω, which can be attributed to the presence of PAF. However, the impedance of PAF-Li|LFP full-cell LIB has dropped to 35 Ω after 5 cycles (Fig. 5b). In subsequent cycles, the impedance of Li|LFP full-cell LIB increased, whereas the impedance of PAF-Li|LFP full-cell LIB remained similar. One should note that the increase in impedance can be attributed to the parasite reactions between Li metal and electrolyte, resulting in SEI growth. The stable impedance of PAF-protected Li anode indicates that the presence of an artificial SEI avoids the abovementioned problems.

#### 4 Conclusions

In summary, we have demonstrated that a composite membrane, composed of inorganic and organic components, effectively protects the Li metal anode during electrochemical cycling by hindering the dendritic growth and suppressing the side reactions. The PAF composite film, with PVDF-HFP to AlPO<sub>4</sub> mass ratio of 9:1 and a thickness of 8.5 μm, exhibited Young's modulus of 1.6 GPa, which is far higher than a typical SEI (≈ 150 MPa).

Moreover, full-cell Li-ion battery was constructed by using LiFePO<sub>4</sub> cathode and PAF-protected Li anode, which rendered a high specific capacity of 148.1 mAh g<sup>-1</sup> and excellent capacity retention of 90% after 400 charge/discharge cycles. The results reveal that PAF-protected Li anodes exhibited a low overpotential of 375 mV and stable cycling performance (> 1000 h) under a high current density of 3 mA cm<sup>-2</sup> and high areal capacity of 2 mAh cm<sup>-2</sup>. Thus, we anticipate that the design of an organic–inorganic hybrid



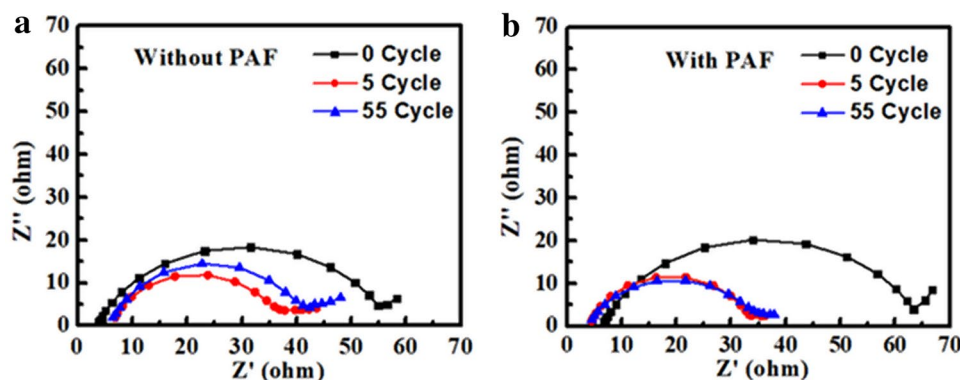


**Fig. 5** Electrochemical impedance spectra of **a** Li/LFP full-cell LIB and **b** PAF-Li/LFP full-cell LIB after charge/discharge cycling at 1 C

artificial protective film is an industrially viable option for the development of next-generation secondary Li batteries.

#### Abbreviations

Al: Aluminum; C: Carbon; DOL: 1,3-dioxolane; DME: 1,2-dimethoxyethane; EDS: Energy dispersive spectroscopy; F: Fluorine; Li: Lithium; LiTFSI: Lithium bis(trifluoromethanesulfonyl) imide; LFP:  $\text{LiFePO}_4$ ; LMBs: Lithium metal batteries; O: Oxygen; P: Phosphorus; PVDF – HFP: Poly(vinylidene fluoride-co-hexafluoropropylene); PAF: PVDF-HFP/nano- $\text{AlPO}_4$  composite film; SEI: Solid electrolyte interphase; XRD: X-ray diffraction.

#### Acknowledgements

Research at Argonne National Laboratory was supported by U.S. Department of Energy (DOE), Vehicle Technologies Office. Argonne National Laboratory is operated for the US Department of Energy by U Chicago Argonne, LLC, under contract DE-AC02-06CH11357. The authors thank Joint Work Plan for Research Projects under the Clean Vehicles Consortium at U.S. and China–Clean Energy Research Center (CERC–CVC2.0, 2016–2020). Moreover, authors would like to acknowledge the support from Tsinghua University-Zhangjiagang Joint Institute for Hydrogen Energy and Lithium-Ion Battery Technology (JHILT).

#### Authors' contributions

All authors have participated in analyzing data and writing the manuscript. All authors read and approved the final manuscript.

#### Funding

We acknowledge the support from the Ministry of Science and Technology of China (No. 2019YFE0100200 and 2019YFA0705703), the Tsinghua University Initiative Scientific Research Program (No. 2019Z02UTY06), the National Natural Science Foundation of China (No. U1564205) and the Beijing Municipal Program (Grant No. YETP0157).

#### Availability of data and materials

The test materials and data are available from the corresponding author on reasonable request.

#### Competing interests

The authors declare that they have no competing interests.

#### Author details

<sup>1</sup> College of Chemical Engineering, Beijing University of Chemical Technology, Beijing 100029, People's Republic of China. <sup>2</sup> Institute of Nuclear & New Energy Technology, Tsinghua University, Beijing 100084, People's Republic of China. <sup>3</sup> Beijing Guyue New Materials Research Institute, Beijing University of Technology, Beijing 100124, China. <sup>4</sup> Chemical Sciences and Engineering Division, Argonne National Laboratory, Argonne, IL 60439, USA. <sup>5</sup> State Key Laboratory of Automotive safety and Energy, Tsinghua University, Beijing 100084, People's

Republic of China. <sup>6</sup> School of Chemical Engineering, Beijing Institute of Petrochemical Technology, Beijing 100176, People's Republic of China.

Received: 12 March 2020 Accepted: 2 June 2020

Published online: 15 June 2020

#### References

1. E.C. Evans, Lithium batteries: to the limits of lithium. *Nature* **526**, S93 (2015)
2. X.B. Cheng, R. Zhang, C.Z. Zhao, F. Wei, J.G. Zhang, Q. Zhang, A review of solid electrolyte interphases on lithium metal anode. *Adv. Sci.* **3**, 1500213 (2016)
3. X.-B. Cheng, R. Zhang, C.-Z. Zhao, Q. Zhang, Toward safe lithium metal anode in rechargeable batteries: a review. *Chem. Rev.* **117**, 10403–10473 (2017)
4. D. Lin, Y. Liu, Y. Cui, Reviving the lithium metal anode for high-energy batteries. *Nat. Nanotechnol.* **12**, 194 (2017)
5. W. Xu, J.L. Wang, F. Ding, X.L. Chen, E. Nasybutin, Y.H. Zhang, J.G. Zhang, Lithium metal anodes for rechargeable batteries. *Energy. Environ. Sci.* **7**, 513–537 (2014)
6. M.D. Tikekar, S. Choudhury, Z.Y. Tu, L.A. Archer, Design principles for electrolytes and interfaces for stable lithium-metal batteries. *Nature. Energy* **1**, 1–7 (2016)
7. J.-M. Tarascon, M. Armand, Issues and challenges facing rechargeable lithium batteries, *Materials for Sustainable Energy*, pp. 171–179
8. J.B. Goodenough, Y. Kim, Challenges for rechargeable li batteries. *Chem. Mater.* **22**, 587–603 (2010)
9. P.-Y. Zhai, H.-J. Peng, X.-B. Cheng, L. Zhu, J.-Q. Huang, W. Zhu, Q. Zhang, Scaled-up fabrication of porous-graphene-modified separators for high-capacity lithium–sulfur batteries. *Energy. Storage. Mat.* **7**, 56–63 (2017)
10. A. Ben-Naim, D. Casadei, Modern thermodynamics. *MRS. Bull.* **42**, 857–858 (2017)
11. X.B. Cheng, Q. Zhang, Growth mechanisms and suppression strategies of lithium metal dendrites. *Prog. Chem* **30**, 51–72 (2018)
12. D. Rehnlund, C. Ihrfors, J. Maibach, L. Nyholm, Dendrite-free lithium electrode cycling via controlled nucleation in low  $\text{LiPF}_6$  concentration electrolytes. *Mater. Today* **21**, 1010–1018 (2018)
13. A. Jana, R.E. Garcia, Lithium dendrite growth mechanisms in liquid electrolytes. *Nano. Energy* **41**, 552–565 (2017)
14. J. Qian, W. Xu, P. Bhattacharya, M. Engelhard, W.A. Henderson, Y. Zhang, J.-G. Zhang, Dendrite-free Li deposition using trace-amounts of water as an electrolyte additive. *Nano. Energy* **15**, 135–144 (2015)
15. J.W. Xiang, Y. Zhao, L.X. Yuan, C.J. Chen, Y. Shen, F. Hu, Z.X. Hao, J. Liu, B.X. Xu, Y.H. Huang, A strategy of selective and dendrite-free lithium deposition for lithium batteries. *Nano. Energy* **42**, 262–268 (2017)
16. M. Ye, Y. Xiao, Z. Cheng, L. Cui, L. Jiang, L. Qu, A smart, anti-piercing and eliminating-dendrite lithium metal battery. *Nano. Energy* **49**, 403–410 (2018)

17. Y.C. Zhou, Z.J. Li, Y.C. Lu, A stable lithium-selenium interface via solid/liquid hybrid electrolytes: blocking polyselenides and suppressing lithium dendrite. *Nano. Energy* **39**, 554–561 (2017)
18. Y.H. Zhang, J.F. Qian, W. Xu, S.M. Russell, X.L. Chen, E. Nasybulin, P. Bhattacharya, M.H. Engelhard, D.H. Mei, R.G. Cao, F. Ding, A.V. Cresce, K. Xu, J.G. Zhang, Dendrite-free lithium deposition with self-aligned nanorod structure. *Nano. Lett.* **14**, 6889–6896 (2014)
19. T.T. Zuo, Y.X. Yin, S.H. Wang, P.F. Wang, X.N. Yang, J. Liu, C.P. Yang, Y.G. Guo, Trapping lithium into hollow silica microspheres with a carbon nanotube core for dendrite-free lithium metal anodes. *Nano. Lett.* **18**, 297–301 (2018)
20. X.L. Ji, D.Y. Liu, D.G. Prendiville, Y.C. Zhang, X.N. Liu, G.D. Stucky, Spatially heterogeneous carbon-fiber papers as surface dendrite-free current collectors for lithium deposition. *Nano. Today* **7**, 10–20 (2012)
21. H. Wang, M. Matsui, H. Kuwata, H. Sonoki, Y. Matsuda, X. Shang, Y. Takeda, O. Yamamoto, N. Imanishi, A reversible dendrite-free high-areal-capacity lithium metal electrode. *Nat. Commun* **8**, 15106 (2017)
22. P. Zou, Y. Wang, S.W. Chiang, X. Wang, F. Kang, C. Yang, Directing lateral growth of lithium dendrites in micro-compartmented anode arrays for safe lithium metal batteries. *Nat. Commun* **9**, 464 (2018)
23. M.J. Zachman, Z. Tu, S. Choudhury, L.A. Archer, L.F. Kourkoutis, Cryo-STEM mapping of solid-liquid interfaces and dendrites in lithium-metal batteries. *Nature* **560**, 345–349 (2018)
24. Y. Liu, D. Lin, Z. Liang, J. Zhao, K. Yan, Y. Cui, Lithium-coated polymeric matrix as a minimum volume-change and dendrite-free lithium metal anode. *Nat Commun* **7**, 10992 (2016)
25. Y. Liu, Q. Liu, L. Xin, Y. Liu, F. Yang, E.A. Stach, J. Xie, Making Li-metal electrodes rechargeable by controlling the dendrite growth direction. *Nature Energy* **2**, 17083 (2017)
26. Q. Pang, A. Shyamsunder, B. Narayanan, C.Y. Kwok, L.A. Curtiss, L.F. Nazar, Tuning the electrolyte network structure to invoke quasi-solid state sulfur conversion and suppress lithium dendrite formation in Li-S batteries. *Nature Energy* **3**, 783–791 (2018)
27. K.J. Harry, D.T. Hallinan, D.Y. Parkinson, A.A. MacDowell, N.P. Balsara, Detection of subsurface structures underneath dendrites formed on cycled lithium metal electrodes. *Nat. Mater.* **13**, 69–73 (2014)
28. C.Z. Zhao, X.Q. Zhang, X.B. Cheng, R. Zhang, R. Xu, P.Y. Chen, H.J. Peng, J.Q. Huang, Q. Zhang, An anion-immobilized composite electrolyte for dendrite-free lithium metal anodes. *Proc. Natl. Acad. Sci. USA*. **114**, 11069–11074 (2017)
29. L. Li, S. Basu, Y. Wang, Z. Chen, P. Hundekar, B. Wang, J. Shi, Y. Shi, S. Narayanan, N. Koratkar, Self-heating-induced healing of lithium dendrites. *Science* **359**, 1513–1516 (2018)
30. W. Zhang, H.L. Zhuang, L. Fan, L. Gao, Y. Lu, A “cation-anion regulation” synergistic anode host for dendrite-free lithium metal batteries. *Sci. Adv.* **4**(2), eaar4410 (2018)
31. C.Z. Zhao, P.Y. Chen, R. Zhang, X. Chen, B.Q. Li, X.Q. Zhang, X.B. Cheng, Q. Zhang, An ion redistributor for dendrite-free lithium metal anodes. *Sci. Adv.* **4**(11), eaat3446 (2018)
32. X. Li, J. Zheng, X. Ren, M.H. Engelhard, W. Zhao, Q. Li, J.-G. Zhang, W. Xu, Dendrite-free and performance-enhanced lithium metal batteries through optimizing solvent compositions and adding combinational additives. *Adv. Energy. Mater* **8**, 1703022 (2018)
33. J.S. Lee, H. Kim, C. Jo, J. Jeong, J. Ko, S. Han, M.S. Lee, H.-Y. Lee, J.W. Han, J. Lee, J.B. Lee, Enzyme-driven Hasselback-like DNA-based inorganic superstructures. *Adv. Func. Mater.* **27**, 1704213 (2017)
34. T.T. Dong, J.J. Zhang, G.J. Xu, J.C. Chai, H.P. Du, L.L. Wang, H.J. Wen, X. Zang, A.B. Du, Q.M. Jia, X.H. Zhou, G.L. Cui, A multifunctional polymer electrolyte enables ultra-long cycle-life in a high-voltage lithium metal battery. *Energy. Environ. Sci.* **11**, 1197–1203 (2018)
35. F. Ding, W. Xu, G.L. Graff, J. Zhang, M.L. Sushko, X. Chen, Y. Shao, M.H. Engelhard, Z. Nie, J. Xiao, X. Liu, P.V. Sushko, J. Liu, J.-G. Zhang, Dendrite-Free lithium deposition via self-healing electrostatic shield mechanism. *J. Am. Chem. Soc.* **135**, 4450–4456 (2013)
36. S.H. Jiao, X.D. Ren, R.G. Cao, M.H. Engelhard, Y.Z. Liu, D.H. Hu, D.H. Mei, J.M. Zheng, W.G. Zhao, Q.Y. Li, N. Liu, B.D. Adams, C. Ma, J. Liu, J.G. Zhang, W. Xu, Stable cycling of high-voltage lithium metal batteries in ether electrolytes. *Nat. Energy* **3**, 739–746 (2018)
37. J.M. Zheng, M.H. Engelhard, D.H. Mei, S.H. Jiao, B.J. Polzin, J.G. Zhang, W. Xu, Electrolyte additive enabled fast charging and stable cycling lithium metal batteries. *Nat. Energy* **2**, 8 (2017)
38. Q. Yun, Y.-B. He, W. Lv, Y. Zhao, B. Li, F. Kang, Q.-H. Yang, Chemical dealloying derived 3D porous current collector for Li metal anodes. *Adv. Mater.* **28**, 6932–6939 (2016)
39. C.-P. Yang, Y.-X. Yin, S.-F. Zhang, N.-W. Li, Y.-G. Guo, Accommodating lithium into 3D current collectors with a submicron skeleton towards long-life lithium metal anodes. *Nat. Commun* **6**, 8058 (2015)
40. C. Zhang, W. Lv, G. Zhou, Z. Huang, Y. Zhang, R. Lyu, H. Wu, Q. Yun, F. Kang, Q.-H. Yang, Vertically aligned lithiophilic CuO nanosheets on a Cu collector to stabilize lithium deposition for lithium metal batteries. *Adv Energy Mat* **8**, 1703404 (2018)
41. H. Zhao, D. Lei, Y.-B. He, Y. Yuan, Q. Yun, B. Ni, W. Lv, B. Li, Q.-H. Yang, F. Kang, J. Lu, Compact 3D copper with uniform porous structure derived by electrochemical dealloying as dendrite-free lithium metal anode current collector. *Adv. Energy. Mat* **8**, 1800266 (2018)
42. S. Liu, X. Xia, Y. Zhong, S. Deng, Z. Yao, L. Zhang, X.-B. Cheng, X. Wang, Q. Zhang, J. Tu, 3D TiC/C core/shell nanowire skeleton for dendrite-free and long-life lithium metal anode. *Adv. Energy. Mater.* **8**, 1702322 (2018)
43. S.-S. Chi, Y. Liu, W.-L. Song, L.-Z. Fan, Q. Zhang, Prestoring lithium into stable 3D nickel foam host as dendrite-free lithium metal anode. *Adv. Func. Mater.* **27**, 1700348 (2017)
44. Q. Lu, Y.B. He, Q. Yu, B. Li, Y.V. Kaneti, Y. Yao, F. Kang, Q.H. Yang, Dendrite-free, high-rate, long-life lithium metal batteries with a 3D cross-linked network polymer electrolyte. *Adv. Mater.* **29**, 1604460 (2017)
45. W. Fan, N.W. Li, X. Zhang, S. Zhao, R. Cao, Y. Yin, Y. Xing, J. Wang, Y.G. Guo, C. Li, A dual-salt Gel polymer electrolyte with 3D cross-linked polymer network for dendrite-free lithium metal batteries. *Adv. Sci* **5**, 1800559 (2018)
46. C.P. Yang, L. Zhang, B.Y. Liu, S.M. Xu, T. Hamann, D. McOwen, J.Q. Dai, W. Luo, Y.H. Gong, E.D. Wachsman, L.B. Hu, Continuous plating/stripping behavior of solid-state lithium metal anode in a 3D ion-conductive framework. *Proc. Natl. Acad. Sci. USA* **115**, 3770–3775 (2018)
47. Y. Liu, D. Lin, P.Y. Yuen, K. Liu, J. Xie, R.H. Dauskardt, Y. Cui, An artificial solid electrolyte interphase with high Li-Ion conductivity, mechanical strength, and flexibility for stable lithium metal anodes. *Adv. Mater.* **29**, 1605331 (2017)
48. S.M. Wood, C.H. Pham, R. Rodriguez, S.S. Nathan, A.D. Dolocan, H. Celio, J.P. de Souza, K.C. Klavetter, A. Heller, C.B. Mullins, K + Reduces lithium dendrite growth by forming a thin, less-resistive solid electrolyte interphase. *Acs. Energy. Lett.* **1**, 414–419 (2016)
49. D. Zhou, R.L. Liu, Y.B. He, F.Y. Li, M. Liu, B.H. Li, Q.H. Yang, Q. Cai, F.Y. Kang, SiO<sub>2</sub> hollow nanosphere-based composite solid electrolyte for lithium metal batteries to suppress lithium dendrite growth and enhance cycle life. *Adv Energy Mater* **6**, 1502214 (2016)
50. L. Fan, S. Chen, J. Zhu, R. Ma, S. Li, R. Podila, A.M. Rao, G. Yang, C. Wang, Q. Liu, Z. Xu, L. Yuan, Y. Huang, B. Lu, Simultaneous suppression of the dendrite formation and shuttle effect in a lithium-Sulfur battery by bilateral solid electrolyte interface. *Adv. Sci.* **5**, 1700934 (2018)
51. B. Wu, S. Wang, J. Lochala, D. Desrochers, B. Liu, W. Zhang, J. Yang, J. Xiao, The role of the solid electrolyte interphase layer in preventing Li dendrite growth in solid-state batteries. *Energy. Environ. Sci.* **11**, 1803–1810 (2018)
52. C. Shen, H.B. Yan, J.L. Gu, Y.L. Gao, J.J. Yang, K.Y. Xie, Li<sub>2</sub>O-Reinforced solid electrolyte interphase on three-dimensional sponges for dendrite-free lithium deposition. *Front. Chem* **6**, 517 (2018)
53. X.B. Cheng, Q. Zhang, Dendrite-free lithium metal anodes: stable solid electrolyte interphases for high-efficiency batteries. *J. Mater. Chem. A*. **3**, 7207–7209 (2015)
54. M. Zier, F. Scheiba, S. Oswald, J. Thomas, D. Goers, T. Scherer, M. Klose, H. Ehrenberg, J. Eckert, Lithium dendrite and solid electrolyte interphase investigation using OsO<sub>4</sub>. *J. Power. Sour.* **266**, 198–207 (2014)
55. J. Zhang, R. Wang, X. Yang, W. Lu, X. Wu, X. Wang, H. Li, L. Chen, Direct observation of inhomogeneous solid electrolyte interphase on MnO anode with atomic force microscopy and spectroscopy. *Nano. Lett.* **12**, 2153–2157 (2012)
56. F.F. Shi, A. Pei, D.T. Boyle, J. Xie, X.Y. Yu, X.K. Zhang, Y. Cui, Lithium metal stripping beneath the solid electrolyte interphase. *Proc. Natl. Acad. Sci. USA*. **115**, 8529–8534 (2018)
57. W. Liu, W.Y. Li, D. Zhuo, G.Y. Zheng, Z.D. Lu, K. Liu, Y. Cui, Core-shell nanoparticle coating as an interfacial layer for dendrite free lithium metal anodes. *Acs. Cent. Sci* **3**, 135–140 (2017)

58. C. Yan, X.B. Cheng, Y. Tian, X. Chen, X.Q. Zhang, W.J. Li, J.Q. Huang, Q. Zhang, Dual-layered film protected lithium metal anode to enable dendrite-free lithium deposition. *Adv. Mater.* **30**, 1707629 (2018)
59. L. Ma, M.S. Kim, L.A. Archer, Stable artificial solid electrolyte interphases for lithium batteries. *Chem. Mater.* **29**, 4181–4189 (2017)
60. R. Xu, X.-Q. Zhang, X.-B. Cheng, H.-J. Peng, C.-Z. Zhao, C. Yan, J.-Q. Huang, Artificial soft-rigid protective layer for dendrite-free lithium metal anode. *Adv. Func. Mater.* **28**, 1705838 (2018)
61. L. Wang, L. Zhang, Q. Wang, W. Li, B. Wu, W. Jia, Y. Wang, J. Li, H. Li, Long lifespan lithium metal anodes enabled by Al<sub>2</sub>O<sub>3</sub> sputter coating. *Energy. Stor. Mater.* **10**, 16–23 (2018)
62. H.-K. Jing, L.-L. Kong, S. Liu, G.-R. Li, X.-P. Gao, Protected lithium anode with porous Al<sub>2</sub>O<sub>3</sub> layer for lithium–sulfur battery. *J. Mater. Chem. A* **3**, 12213–12219 (2015)
63. L. Chen, J.G. Connell, A. Nie, Z. Huang, K.R. Zavadil, K.C. Klavetter, Y. Yuan, S. Sharifi-Asl, R. Shahbazian-Yassar, J.A. Libera, A.U. Mane, J.W. Elam, Lithium metal protected by atomic layer deposition metal oxide for high performance anodes. *J. Mater. Chem. A* **5**, 12297–12309 (2017)
64. A.C. Kozen, C.-F. Lin, A.J. Pearse, M.A. Schroeder, X. Han, L. Hu, S.-B. Lee, G.W. Rubloff, M. Noked, Next-generation lithium metal anode engineering via atomic layer deposition. *ACS Nano* **9**, 5884–5892 (2015)
65. M.D. Tikekar, L.A. Archer, D.L. Koch, Stabilizing electrodeposition in elastic solid electrolytes containing immobilized anions. *Sci. Adv.* **2**, e1600320 (2016)
66. S.M. Choi, I.S. Kang, Y.-K. Sun, J.-H. Song, S.-M. Chung, D.-W. Kim, Cycling characteristics of lithium metal batteries assembled with a surface modified lithium electrode. *J. Power. Sour.* **244**, 363–368 (2013)
67. F. Wu, J. Qian, R. Chen, J. Lu, L. Li, H. Wu, J. Chen, T. Zhao, Y. Ye, K. Amine, An effective approach to protect lithium anode and improve cycle performance for Li–S batteries. *ACS. Appl. Mater. Interfaces.* **6**, 15542–15549 (2014)
68. S.Y. Wei, S. Choudhury, Z.Y. Tu, K.H. Zhang, L.A. Archer, Electrochemical interphases for high-energy storage using reactive metal anodes. *Accounts. Chem. Res.* **51**, 80–88 (2018)
69. D.J. Lee, H. Lee, Y.-J. Kim, J.-K. Park, H.-T. Kim, Sustainable redox mediation for lithium-oxygen batteries by a composite protective layer on the lithium-metal anode. *Adv. Mater.* **28**, 857–863 (2016)
70. X. Liang, Q. Pang, I.R. Kochetkov, M.S. Sempere, H. Huang, X. Sun, L.F. Nazar, A facile surface chemistry route to a stabilized lithium metal anode. *Nat. Energy.* **2**, 17119 (2017)
71. X.B. Cheng, T.Z. Hou, R. Zhang, H.J. Peng, C.Z. Zhao, J.Q. Huang, Q. Zhang, Dendrite-free lithium deposition induced by uniformly distributed lithium ions for efficient lithium metal batteries. *Adv. Mater.* **28**, 2888–2895 (2016)
72. P.C. Shi, L.C. Zhang, H.F. Xiang, X. Liang, Y. Sun, W. Xu, Lithium difluorophosphate as a dendrite-suppressing additive for lithium metal batteries. *ACS. Appl. Mater. Interfaces.* **10**, 22201–22209 (2018)
73. M. Bai, K. Xie, K. Yuan, K. Zhang, N. Li, C. Shen, Y. Lai, R. Vajtai, P. Ajayan, B. Wei, A scalable approach to dendrite-free lithium anodes via spontaneous reduction of spray-coated graphene oxide layers. *Adv. Mater.* **30**, e1801213 (2018)
74. K.N. Wood, E. Kazyak, A.F. Chadwick, K.H. Chen, J.G. Zhang, K. Thornton, N.P. Dasgupta, Dendrites and pits: untangling the complex behavior of lithium metal anodes through operando video microscopy. *ACS. Cent. Sci.* **2**, 790–801 (2016)
75. Z.Y. Tu, Y. Kambe, Y.Y. Lu, L.A. Archer, Nanoporous polymer-ceramic composite electrolytes for lithium metal batteries. *Adv. Energy. Mater.* **4**, 1300654 (2014)
76. Z.Y. Tu, L. Archer, Stabilizing lithium electrodeposition using high conductivity/modulus nanoporous hybrid electrolyte for high energy metal-based batteries. *Abstr. Pap. Am. Chem. S.* (2017). <https://doi.org/10.1002/aenm.201602367>
77. Z. Tu, P. Nath, Y. Lu, M.D. Tikekar, L.A. Archer, Nanostructured electrolytes for stable lithium electrodeposition in secondary batteries. *Acc. Chem. Res.* **48**, 2947–2956 (2015)
78. Y. Lu, Z. Tu, L.A. Archer, Stable lithium electrodeposition in liquid and nanoporous solid electrolytes. *Nat. Mater.* **13**, 961–969 (2014)
79. J. Cao, Y. Shang, L. Wang, X. He, L. Deng, H. Chen, Composite electrospun membranes containing a monodispersed nano-sized TiO<sub>2</sub>@Li+ single ionic conductor for Li-ion batteries. *RSC. Adv.* **5**, 8258–8262 (2015)
80. J. Cao, L. Wang, M. Fang, X.M. He, J.J. Li, J. Gao, L.F. Deng, J.L. Wang, H. Chen, Structure and electrochemical properties of composite polymer electrolyte based on poly(vinylidene fluoride-hexafluoropropylene)/titania-poly(methyl methacrylate) for lithium-ion batteries. *J. Power. Sour.* **246**, 499–504 (2014)
81. J. Cao, L. Wang, M. Fang, Y. Shang, L. Deng, J. Yang, J. Li, H. Chen, X. He, Interfacial compatibility of gel polymer electrolyte and electrode on performance of Li-ion battery. *Electrochim. Acta* **114**, 527–532 (2013)
82. J. Cao, L. Wang, X.M. He, M. Fang, J. Gao, J.J. Li, L.F. Deng, H. Chen, G.Y. Tian, J.L. Wang, S.S. Fan, In situ prepared nano-crystalline TiO<sub>2</sub>-poly(methyl methacrylate) hybrid enhanced composite polymer electrolyte for Li-ion batteries. *J. Mater. Chem. A* **1**, 5955–5961 (2013)
83. J. Cao, L. Wang, Y.M. Shang, M. Fang, L.F. Deng, J. Gao, J.J. Li, H. Chen, X.M. He, Dispersibility of nano-TiO<sub>2</sub> on performance of composite polymer electrolytes for Li-ion batteries. *Electrochim. Acta.* **111**, 674–679 (2013)
84. Y. Wu, H. Ming, M. Li, J. Zhang, W. Wahyudi, L. Xie, X. He, J. Wang, Y. Wu, J. Ming, New organic complex for lithium layered oxide modification: ultrathin coating, high-voltage, and safety performances. *ACS. Energy. Lett.* **4**, 656–665 (2019)
85. J. Lang, Y. Long, J. Qu, X. Luo, H. Wei, K. Huang, H. Zhang, L. Qi, Q. Zhang, Z. Li, H. Wu, One-pot solution coating of high quality LiF layer to stabilize Li metal anode. *Energy. Storage. Mater.* **16**, 85–90 (2019)
86. T. Osaka, M. Kitahara, Y. Uchida, T. Momma, K. Nishimura, Improved morphology of plated lithium in poly(vinylidene fluoride) based electrolyte. *J. Power. Sour.* **81–82**, 734–738 (1999)
87. Y. Xia, X. Wang, X. Xia, R. Xu, S. Zhang, J. Wu, Y. Liang, C. Gu, J. Tu, A newly designed composite gel polymer electrolyte based on poly(Vinylidene Fluoride-Hexafluoropropylene) (PVDF-HFP) for enhanced solid-state lithium-sulfur batteries. *A. Chem. A. Eur. J.* **23**, 15203–15209 (2017)
88. H.T.T. Le, D.T. Ngo, R.S. Kalubarme, G. Cao, C.-N. Park, C.-J. Park, Composite gel polymer electrolyte based on poly(vinylidene fluoride-hexafluoropropylene) (PVDF-HFP) with modified aluminum-doped lithium lanthanum titanate (A-LLTO) for high-performance lithium rechargeable batteries. *ACS. Appl. Mater. Interfaces.* **8**, 20710–20719 (2016)
89. H.P. Wang, H.T. Huang, S.L. Wunder, Novel microporous poly(vinylidene fluoride) blend electrolytes for lithium-ion batteries. *J. Electrochem. Soc.* **147**, 2853–2861 (2000)
90. M. Spasova, N. Manolova, N. Markova, I. Rashkov, Tuning the properties of PVDF or PVDF-HFP fibrous materials decorated with ZnO nanoparticles by applying electrospinning alone or in conjunction with electrospraying. *Fibers. Polym.* **18**, 649–657 (2017)
91. C.-H. Du, B.-K. Zhu, Y.-Y. Xu, The effects of quenching on the phase structure of vinylidene fluoride segments in PVDF-HFP copolymer and PVDF-HFP/PMMA blends. *J. Mater. Sci.* **41**, 417–421 (2006)

## Publisher's Note

Springer Nature remains neutral with regard to jurisdictional claims in published maps and institutional affiliations.